Available online at www.sciencedirect.com
SCIENCE DIRECT
Polymer 46 (2005) 3425–3439
polymer
www.elsevier.com/locate/polymer

The effect of copolymer composition on the spatial structural hierarchy developed in injection molded bacterial poly(3-hydroxybutyrate-*co*-3-hydroxyvalerate) parts

M. Cakmak[a,*], M. Ghanem[a], T. Yamamoto[b]

[a]*Polymer Engineering Institute, University of Akron, Akron OH 44325-0301, USA*
[b]*Department of Textiles, Industrial Research Institute of Ishikawa and Department of Textiles and Human Life Technology 2-1, Kuratsuki, Kanazawa, Ishikawa, 920-8203 Japan*

Received 13 May 2004; received in revised form 1 December 2004; accepted 8 February 2005
Available online 21 March 2005

Abstract

The effects of copolymer composition on structure development in injection molded bacterial poly(3-hydroxybutyrate-*co*-3-hydroxyvalerate)(PHBHV) parts were investigated. The increase of hydroxyvalerate co-monomer content lowers the melting temperature as it disrupts the crystalline order as a result, depth variation of melting behavior in the injection molded samples were found to depend primarily on the co monomer composition. At lower HV concentrations, the skin regions were found to exhibit a single melting peak that is also higher than those in the interior of the parts where generally bimodal melting behavior is observed. At higher HV content bimodal melting prevails throughout the injection molded parts including the skin and shear regions. This unusual behavior was attributed to the flow induced crystallization in extended chain formation at the skin and ease of inclusion of HV defects in the HB crystals that formed at slower cooling conditions in the interior creating thinner HV rich crystals with lower melting and thicker HV poor crystals with higher melting peaks.

Depth profiling micro beam wide angle X-ray diffraction studies revealed that these polymers exhibit two distinct orientation behaviors depending on the distance from the surface. At the skin, invariably the chain axes are oriented along the flow direction. Beyond the transition layer located between the shear layer and core, the orientation does not disappear as expected from fast crystallizing polymers but rather preferential orientation of crystals with their *a*-axes along the flow direction was observed. At low HV content, the materials exhibit unusually high preferred orientation behavior throughout the thickness even for thick moldings, resembling the orientation behavior of polymers with low orientation relaxation behavior such as thermotropic liquid crystalline polymers. This is partly attributed to the unusually low injection melt temperature employed in these materials to avoid thermal degradation. The increase of HV content in the copolymers was found to change this $c+a$ type orientation gradient across the thickness to gradual decrease of *c*-axis oriented crystals. This change was attributed to the decrease of crystallizability with the addition of HV and increasing melt fraction in the melt stream as the overall melting temperature decreases with the increase of HV content.

Keywords: Microbeam X-ray; Injection molding; Poly (HB CO HV)

1. Introduction

PHB [1–5], and its copolymers are obtained through bacteria based processes. These polymers are generally crystallizable [6–11], and copolymerization with hydroxy valerate suppresses the crystal growth rates [12–20] and commercial grades typically contain nucleating agent (eg. boron nitride) to accelerate the crystallization process. The presence of the HV units in the copolymer limits, or constrains, the thickness of the crystalline lamellae during crystallization that may lead to appearance of multiple endothermic peaks resulting from multiple crystal populations. There are only limited numbers of studies related to the effect of processing conditions on the development of structure and resulting mechanical, optical and degradation characteristics of the manufactured parts. Wang et al. [20] studied the solid state extrusion of PHB/HV to gain

* Corresponding author.

0032-3861/$ - see front matter © 2005 Elsevier Ltd. All rights reserved.
doi:10.1016/j.polymer.2005.02.071

fundamental understanding about their processability below their melting temperatures. Albertsson [21] attributed the presence double melting peaks in extruded parts to differentiate in lamellar thickness and/or perfection governed by the processing conditions. Melt quenching followed by reheat drawing can yield strong PHB fibers [21]. Application of spin-drawing followed by annealing yield fibers with bimodal crystal orientation [22,23]. In the first crystal population, the chain axes are oriented primarily along the fiber axis and in the second population these chains axes are oriented in the transverse direction to the fiber axis. The tenacity and elongation to break of the fibers improves, whereas Young's modulus increases with the increase in the chain orientation factor.

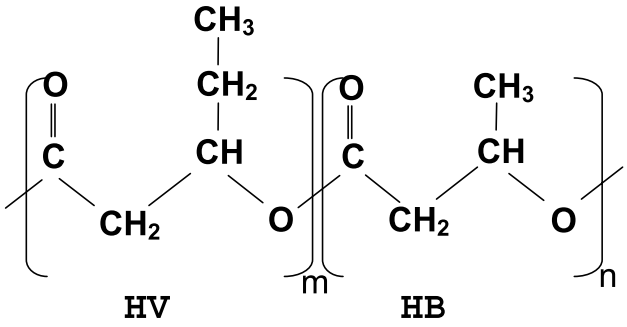

In this experimental study, we focused on the effect of copolymer composition on the structural hierarchy developed in PHBHV injection molded parts.

2. Experimental procedures

2.1. Material

The random copolymers used in this research, (PHBHV) were obtained from Zeneca K. K. As shown in Table 1, three different compositions were used, D300G, D400G, and D600G. All compositions contain boron nitride nucleating agent.

Prior to injection molding, the polymers were dried in vacuum oven for 3 h at 90 °C.

2.2. Injection molding

The PHBHV samples were molded using a Van Dorn 55 type reciprocating screw injection molding machine equipped with an oil-circulating mold temperature controller. The processing conditions of the injection molding in which the samples were prepared are shown in Table 2. The use of such unusually low melt temperature is a common practice.

Table 1
Materials

Grade	Compositions (HV/HB)	Melt flow index[a] (MI)	Melting Temperature (°C)[b]
D300G	5:95	8	159, 167
D400G	8:92	9	142, 159
D600G	12:88	12	142, 152

[a] MI: ASTM 1238-906/2.16 kg at 190 °C.
[b] See procedure in Differential scanning calorimetry section.

Two end gated part geometries were employed in this study: (i) standard ASTM dumbbell with 165 mm. total length and 3.2 mm in thickness, (ii) rectangular prism (60 × 12.7 × 6.3 mm^3). During the injection molding, a hopper dryer system was used.

2.3. Sample sectioning

Since the glass transition temperature of PHBHV copolymers is below room temperature (~0 °C), the structural tests on these samples were performed after sufficient conditioning at room temperature to allow the samples to reach an structural equilibrium state. For this purpose, a section of the molded specimens were cut at the midpoint (#3 location in Fig. 1) with Leco Varicut VC-50 diamond saw. Two cutting procedures were used to further section these samples: in the cutting procedure B the samples were sectioned parallel to the flow direction in the FD-ND plane, along the center of the sample, (Fig. 1). Procedure C consisted of cutting sections from skin to core, parallel to flow direction in the FD-TD plane, as shown in Fig. 2.

2.4. Optical microscopy

2.4.1. Micrographs

The transmission optical photomicrographs of cut samples obtained from procedure B and C, were taken using a Leitz Laborlux 12 POL S microscope with and without λ compensator (530 μm), using Nikon 8008 S camera as well as Sony CCD camera. Samples having

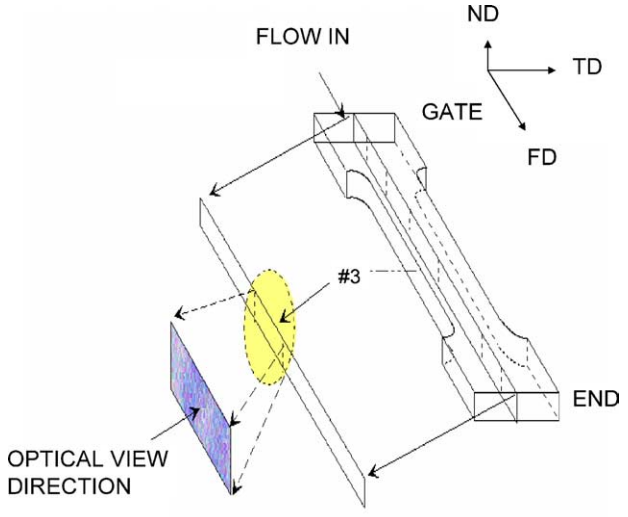

Fig. 1. Cutting procedure B.

Table 2
Molding conditions

Melt temperature (°C)	Mold temperature (°C)	Injection speed (inch/s)	Holding pressure (MPa)	Holding time (sec)
162	25	0.75 and 6.63	1.37	60

average thickness of 10 μm were cut using a Reichert-Jung 2050 microtome for this purpose. These were then sandwiched between two glass slides and placed on the microscope stage so that flow direction is oriented at 45° to both the polarizer and the analyzer.

2.4.2. Hot-stage microscopy

A 10 μm thick microtomed samples obtained from cutting procedure B, were placed between thin cover glass and placed in a Mettler FP82 HT hot stage. The sample was oriented with the flow direction at a 45° angle to the polarization directions of cross-polars of the Leitz microscope. The samples were heated at 2 °C/min in temperature range 26–180 °C. The heating and melting events were recorded with a Sony CCD camera connected to both a video recorder and image-capture card with sun 4/150 workstation.

2.4.3. Birefringence measurement of B-cut samples

4-order Berek compensator was employed to measure the birefringence of the specimens with Leitz Laborlux 12 POL S microscope. The birefringence was measured for poly (3-HB-*co*-3-HV) samples from skin to core on the B-cut samples. Through observation, it was found that the local symmetry axis direction varies with distance from the surface. In order to determine the birefringence, the local direction of the symmetry axis was determined first and birefringence was measured with respect to this local axis. This type of measurement provides the highest local birefringence as it allows measurement of difference in refractive indices in local principal directions.

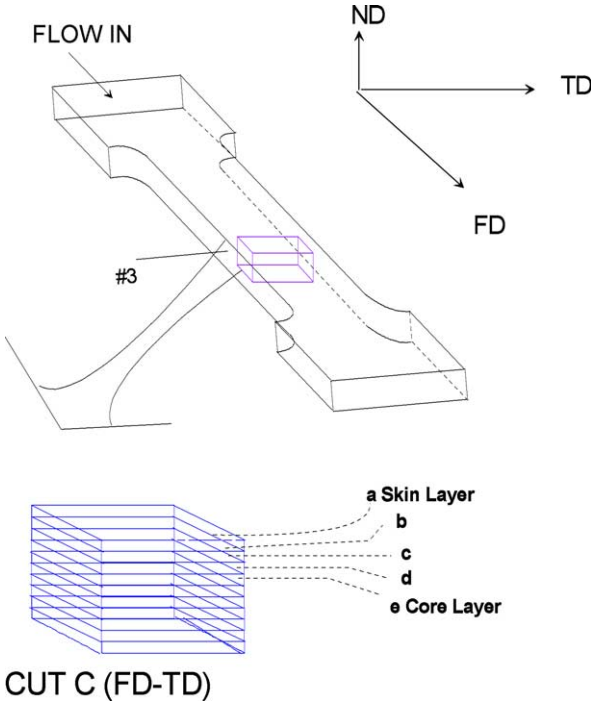

Fig. 2. Cutting procedure C.

The value of optical retardation, Γ (nm), was obtained using the calibration chart provided by the manufacturer of the compensator. The birefringence was then calculated with

$$\Delta n_{12} = \frac{\Gamma}{d}$$

where Γ is the retardation at ($\lambda = 546.1$ nm), d is thickness of the sample (nm).

2.5. Differential scanning calorimetry (DSC)

The thermal analysis of microtomed samples cut with the procedure C was carried out in the temperature ranges 30–200 °C using Perkin–Elmer DSC model 7. About 4 mg samples were weighed and sealed in aluminum pans. Then melting endotherm was obtained at heating rate of 20 °C/min. Since the heat of fusion of the PHB/HV copolymer is not available in the literatures, only $\Delta H_{\exp}$ was considered.

2.6. Wide angle X-ray diffraction (WAXD) studies

2.6.1. Determination of orientation factor

Using the definition of P. H. Hermans [24] for uniaxial orientation factor f, s

$$f_i = \frac{1}{2}(3\langle\cos^2\phi\rangle - 1)$$

where $\langle\cos^2\phi\rangle$ is the mean square cosine) of the angle between a given crystal axis and the fiber axis that serves as the reference direction.

Using Wilchinskys' [25,26] procedure for (110) and (020) crystal planes, $\langle\cos^2\phi_{c,z}\rangle$ for poly(3-hydroxybutyrate-*co*-3-hydroxyvalerate) is expressed as

$$\langle\cos^2\phi_{c,z}\rangle = 1 + \left(\frac{0.076\langle\cos^2\phi_{020,z}\rangle + \langle\cos^2\phi_{110,z}\rangle}{0.536}\right)$$

then, f_b, is directly obtained from data for (020) planes and f_a is obtained from $fa + fc + fc = 0$.

The crystal structure of these polymers is orthorhombic with $a = 9.32$, $b = 10.02$ and $c = 5.52$ as reported by Mitomo et al. [13,18].

2.7. Microbeam X-ray (WAXS)

In order to examine the structural gradient through the thickness direction, Microbeam X-ray (WAXS) patterns of the B-cut were taken at a series of locations from skin to core at #3 location (Fig. 1) using the matrixing microbeam X-ray camera (MMBX) developed in our laboratories [27]. The X-ray beam was directed along the transverse direction for these experiments. The camera was connected to a Rigaku RU-200B rotating anode X-ray generator operated at 40 kV and 150 mA. The Cu Kα X-ray beam, having a 50 μm diameter, was obtained using a nickel foil filter and a pin-hole collimator. A typical exposure time was about 45 min. The film images were digitized using a 12 bit CCD Photometrics camera and non-linearity of film sensitivity was corrected for quantitative evaluation.

2.8. Wide angle X-ray pole figures

To fully describe the crystalline orientation distribution at different depths from skin to core, WAXS pole figure analysis were performed on (110) ($2\theta \sim 13.42°$) and (020) ($2\theta \sim 16.79°$) planes. These values are within 1° of the values for these planes 12.97 and 17.7°2θ based on the crystal structure of Mitomo et al. [18]. For this purpose, a GE XRD-6 generator equipped with an automated quarter circle gonimeter developed in our laboratories was utilized. Small samples of $0.2 \times 0.2 \times 0.2\ mm^3$ in dimensions were cut with the long axis along the flow direction, and were mounted on the quarter circle goniometer with spindle axis parallel to the flow direction. The data were acquired with a computer with $\chi = 5°$ intervals and $\phi = 10°$ intervals. Because of the very small size of the samples, counting times up to 80 s were used to improve the signal-to-noise ratio. Data were plotted as isointensity contour as well as surface maps.

3. Results and discussion

3.1. Thermal characterization

As reported in the literature in great detail, these copolymers are semicrystalline and typically exhibit complex melting behavior depending primarily on chemical composition as well as thermal deformation history they have experienced. The melting temperature decreases with the increase of 3HV comonomer fraction as shown in Fig. 3(a) for P(3HB-*co*-5, 8, 12%-3HV) copolymers. With the increase of HV content the melting peak not only shifts to lower temperatures but also splits into two distinct peaks. At 8% the lower temperature peak becomes dominant and at 12% HV the proportion of the lower melting crystalline species increases. It should be emphasized that the melting peaks of both high and low melting crystallites

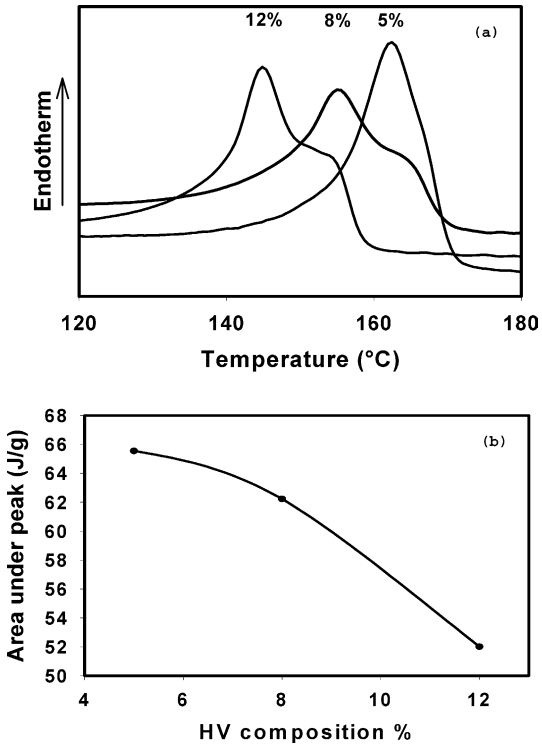

Fig. 3. (a) DSC curves of PHB-*co*-5,8,12% HV as received samples (slices taken from pellets) (b) Area under peak versus HV composition %.

decreases with the increase of HV content clearly indicating the disruptive effects of HV presence in and/or near the crystalline regions.

In addition, the increase in HV fraction in these random copolymers [28] causes reduction in ultimate crystallinities as amply discussed in Ref. [13] (Fig. 3(b)). Mitomo, Barham and Keller [13] suggested that the major fraction of the HV units is excluded from the HB crystal, acting as defect regions thereby disrupting organization of the fold surfaces. In their study, the incorporation of a small fraction of HV in the HB crystals where they act as defects without influencing the lattice spacing also was not ruled out. In addition, Owen et al. [29] research indicated that the higher melting peak corresponds to those crystals that are more perfect devoid of HV defects and the lower melting peaks are very much controlled by other conditions such as heating rate. They proposed two mechanisms for the existence of lower melting peak. In mechanism 1, the lower melting crystals exhibit poor cohesion in the presence of HV defects. In mechanism 2, the lower melting crystals are thin as they were prevented from forming thicker crystals in the presence of HV at their surfaces resulting in presence of lower melting peak. In either mechanism the disruptive effects of HV on melting quite evident. Exclusion of HV to the fold surfaces is inherently requires adequate time in the molten state and is not expected to occur when rapid cooling is employed as in the case of near surfaces in injection molding.

3.2. Injection molded samples

In order to investigate the structural hierarchy variations in the thickness direction in molded samples we elected to section the sample in what is called 'c-cut' procedure depicted at the top of Fig. 2. In this cutting procedure, the sample is sectioned at midpoint between the ends of the injection molded sample. After removal of the edges, it is microtomed into several layers from skin to core and tested in DSC to obtain 'depth profile' of the thermal properties. For 5% HV at low injection speed, the skin region shows only one distinct melting peak. At 300 μm depth the secondary melting peak appears while smaller portion of the higher melting peak still being observable. As the distance from the skin increases the peak at lower temperature increase in size while that of the peak at higher temperature decreases though its peak position eventually shifts to higher temperatures beyond a depth of about 700 μm. Increasing the injection speed essentially produces similar structural gradient across the thickness with slightly lower peak temperature for the low temperature peak as shown in Fig. 4(b).

Increasing the HV content to 8% (Fig. 5) results in a similar melting sequence to that observed for 5% HV with minor variations: In the interior sections of the high speed molded sample, the higher melting peak is located at higher temperatures as compared to that at the skin region while the lower melting peak remaining below that of the latter peak. Further increase of HV content to 12% HV yields a melting sequence in which both low as well as the high melting peaks are observable all the way to the core. At this composition the higher melting peak does not disappear even at the core.

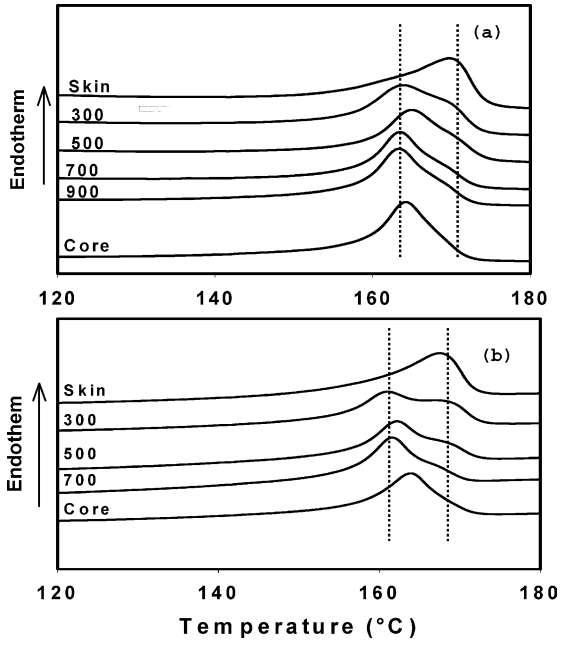

Fig. 4. DSC skin to Core variation of PHB-*co*-5% HV injection molded samples (a) Low speed (0.75 inch/sec). (b) High speed (6.63 inch/sec). Distances are in micrometer scale.

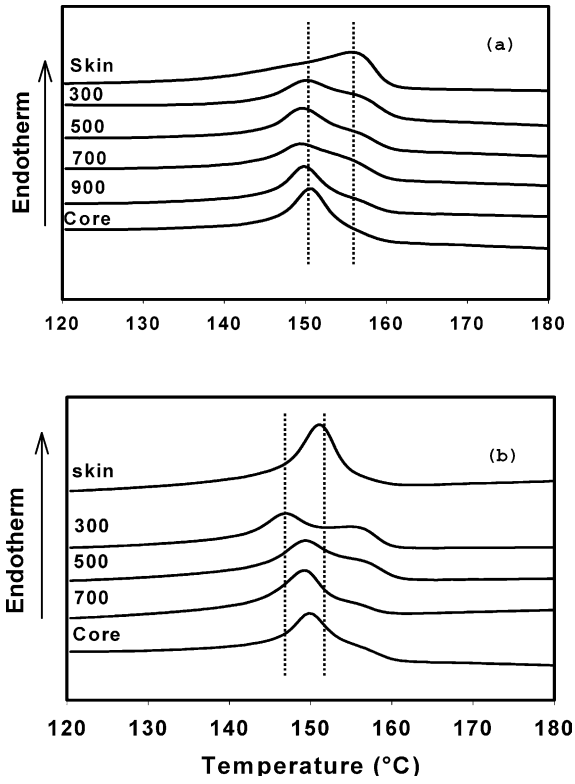

Fig. 5. DSC skin to Core variation of PHB-*co*-8% HV injection molded samples (a) Low speed (0.75 inch/sec). (b) High speed (6.63 inch/sec).

This behavior may be interpreted as follows. During the filling stage, regions nearest to the mold wall experience the fastest cooling rates while the melt is subjected to substantial shearing except at the very surface where the material has just undergone biaxial deformation at the flow front before contacting the mold wall. Under these conditions one expects highly oriented crystals to form even though they are subjected to high cooling rates. This in turn results in observation of this somewhat counterintuitive high melting peak near the skin. In the interior of the parts the lower melting species progressively increase in their population while the higher melting population decreases.

The increase of HV content does not radically change the observations made in 5% HV sample above (Figs. 5 and 6). It is surprising to observe that the lower melting population increases in the interior despite the fact that materials in these regions undergo slower cooling rates during their solidification process. Under these conditions one certainly expects opposite behavior based on commonly understood homopolymer behavior (slower cooling leading to thicker lamellae and higher melting temperature). It appears that slower cooling allows the incorporation of HV defects in the growing crystals or on the surface of the lamellae reducing their melting temperature by one of two mechanisms described above.

In Fig. 7, locations of melting points of each peak were

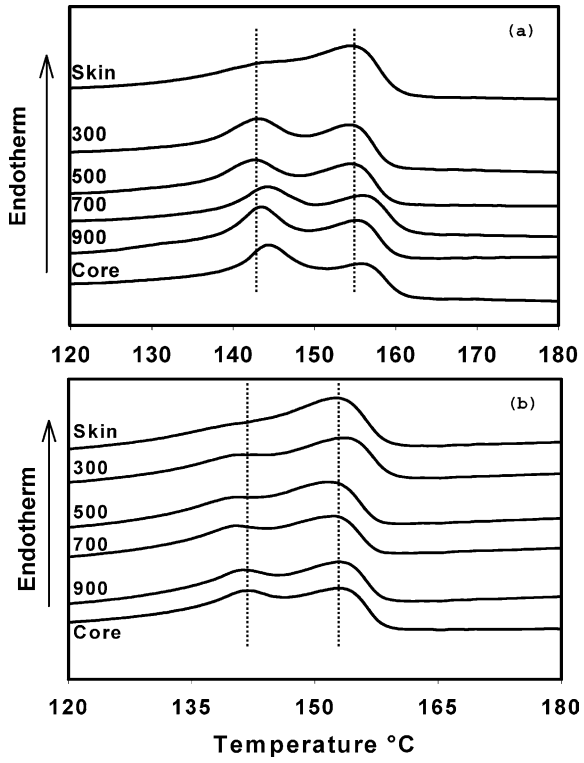

Fig. 6. DSC skin to Core variation of PHB-*co*-12% HV injection molded samples (a) Low speed (0.75 inch/sec). (b) High speed (6.63 inch/sec).

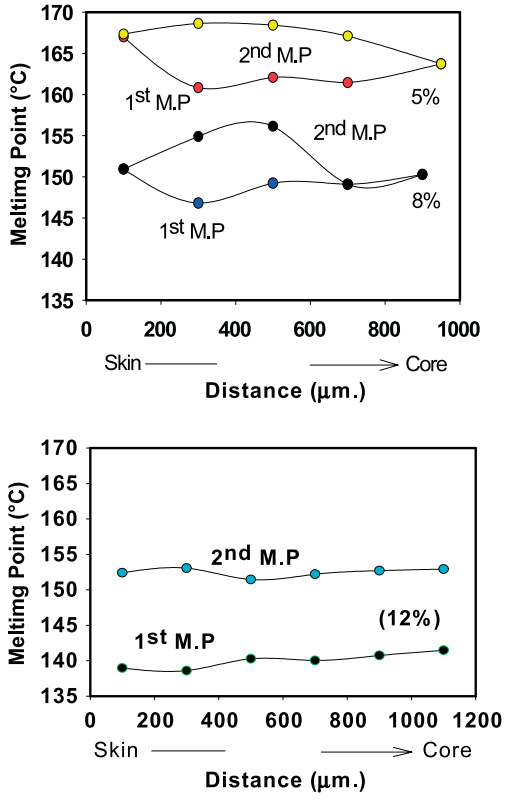

Fig. 7. Depth Variation of melting peak Positions in Injection molded (a) 5% and 8% HV and (b) 12% HV containing copolymers.

plotted as a function of distance from the surface. As illustrated in these figures, single but asymmetric and broad peaks are observed at the skin and core regions while intermediate regions exhibit double melting peaks at 5% and 8% HV concentrations. It should be emphasized that at these compositions, the lower melting peak after having shown a minimum, gradually increases as one approaches the core region while the higher melting peak decreases. We surmise that the higher melting peak represents the extended chain crystallites that form under the influence of flow while the lower melting peaks represent folded lamellar crystals. The fact that higher melting peak disappears towards the interior while the lower melting peak increases attests to these latter mechanisms.

3.3. Hot stage optical microscopy

In order to spatially locate the melting peaks that we observed in different layers and to determine the structural changes occurring during the heating of samples, we performed hot stage video microscopy under crossed polarizers. Fig. 8, shows the melting sequence of thin microtomed B-cut(FD–ND plane) samples taken at mid-point of a dumbbell part molded at high injection speed. The top of each of the optical micrographs represents skin and bottom represent core of the molded parts. The sample was placed in a polarized light microscope between cross polars, with the flow direction making a 45° angle with the

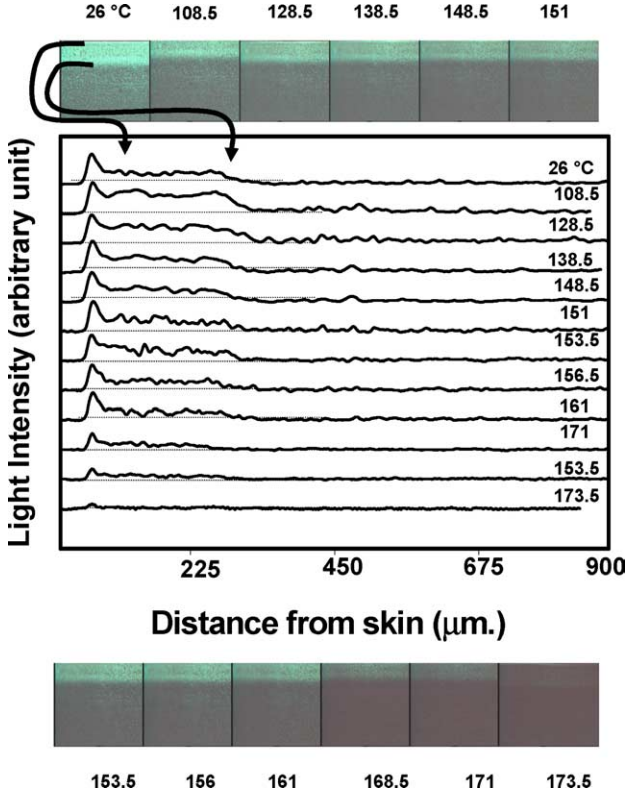

Fig. 8. Cross polarized hot stage optical microscopy of high injection speed molded PHB-*co*-5% HV, (heating rate 2 °C/min).

extension axis of the polarizer and analyzer. The heating rate of 2 °C/min was used in Mettler FP82 hot stage.

Four different morphological layers skin (A), shear (B), transition (C) and core (D) are identified (see Fig. 9 for definitions). We did not observe any significant change in the appearance of these images until around 125 °C. Above this temperature, we observed rearrangement at the core region that manifests as the partial melting of the sub layer. This was followed by the partial melting of the transition layer, then the shear layer in the case of 5% HV and the skin layer with 8% and 12% HV samples. This justifies our earlier suggestion of the presence of two crystal populations melting at different temperatures. The low melting temperature fraction corresponding to those regions where unstable, thin and/or defect filled crystal melts in the early stage, whereas the high melting temperature fraction correspond to highly oriented crystalline regions.

Fig. 9, shows the depolarized light intensity of the skin layer for 5% HV has the highest value and diminishes as the distance is traversed from the surface towards the core region. For 8% HV, the shear region shows higher light intensity than the skin region a behavior attributed to differences in the local orientation of principal axes of the optical indicatrix.

It is important to note that in all samples A curve representing skin regions exhibit increase in the depolarized light intensity above about 120 °C indicating that crystallization is taking place in these regions before they completely disappear. In fact in samples containing 8% and 12% HV we observe multiple peaks in these depolarized intensity profiles. This points to the structural rearrangement processes (either melting of oriented crystals and/or melting and recrystallzation of imperfectly formed crystals formed injection stage.

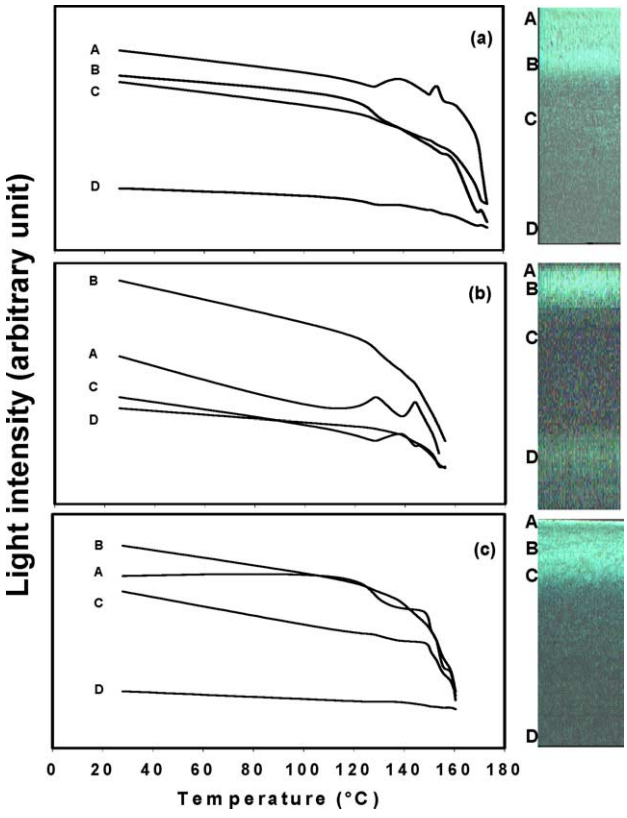

Fig. 9. Variation of optical intensity across the thickness direction during the hot stage optical microscopy melting sequence of (a) PHB-*co*-5% HV (b) PHB-*co*-8% HV (c) PHB-*co*-12% HV.

3.4. Optical microscopy

In fast crystallizing polymer like PE, PP and POM, layer structure of molded parts are usually observed under a cross-polarized microscope. Since PHBHV belongs to this family, we also employed the optical techniques to unravel these structural details. From the moment that the polymer enters the sprue section, the polymer chains experiences severe thermal-deformation gradients.The polymer-chains that establish the skin regions has last seen the extensional flow at the flow front prior to their contact with cold mold and solidify. Therefore they have little time to relax to the random coil state from the acquired orientation levels especially when their melt processing temperatures are set very close to the crystal melting range. These chains in the vicinity of mold surface experience the highest temperature gradient in their solidification.

Because of the poor thermal conductivity exhibited by polymers, the highest cooling rates are usually confined to the boundaries, and the rate of cooling rapidly decreases toward the interior of the parts. During the filling stage, the solid–liquid boundary moves inward sweeping the outer regions of the part near the mold surface mold establishing a very high nucleation density region solidified while undergoing shearing at the solid–liquid interface [30,31]. When the flow front stops moving at the end of the cavity, the boundary between this shear layer and still molten interior layers is established. Depending on the local cooling rates, the polymer crystallizes at decaying cooling rates toward the core with concomitant increase in crystallite sizes.

In order to assess overall optical anisotropy gradient we observed the B-cut samples under crossed polars with the λ plate inserted with its slow axis at 45°. Fig. 10, shows a typical micrograph of samples in FD–ND plane from skin to core. In those regions where the optical subtraction condition is satisfied, one observes yellow, white or gray and those regions that are in addition condition with respect to the slow axis of the lambda plate they appear as blue, green, orange or red depending on the total addition or subtraction, respectively. This technique allows quick assessment of optical anisotropy as a function of position in the thickness direction in these samples.

The intrinsic birefringence of PHB and PHV are -0.076 and -0.056, respectively [32]. Their copolymers should exhibit values between those of two homopolymers. The local symmetry axis orientation and its anisotropy relative to the polarizer and analyzer directions control these

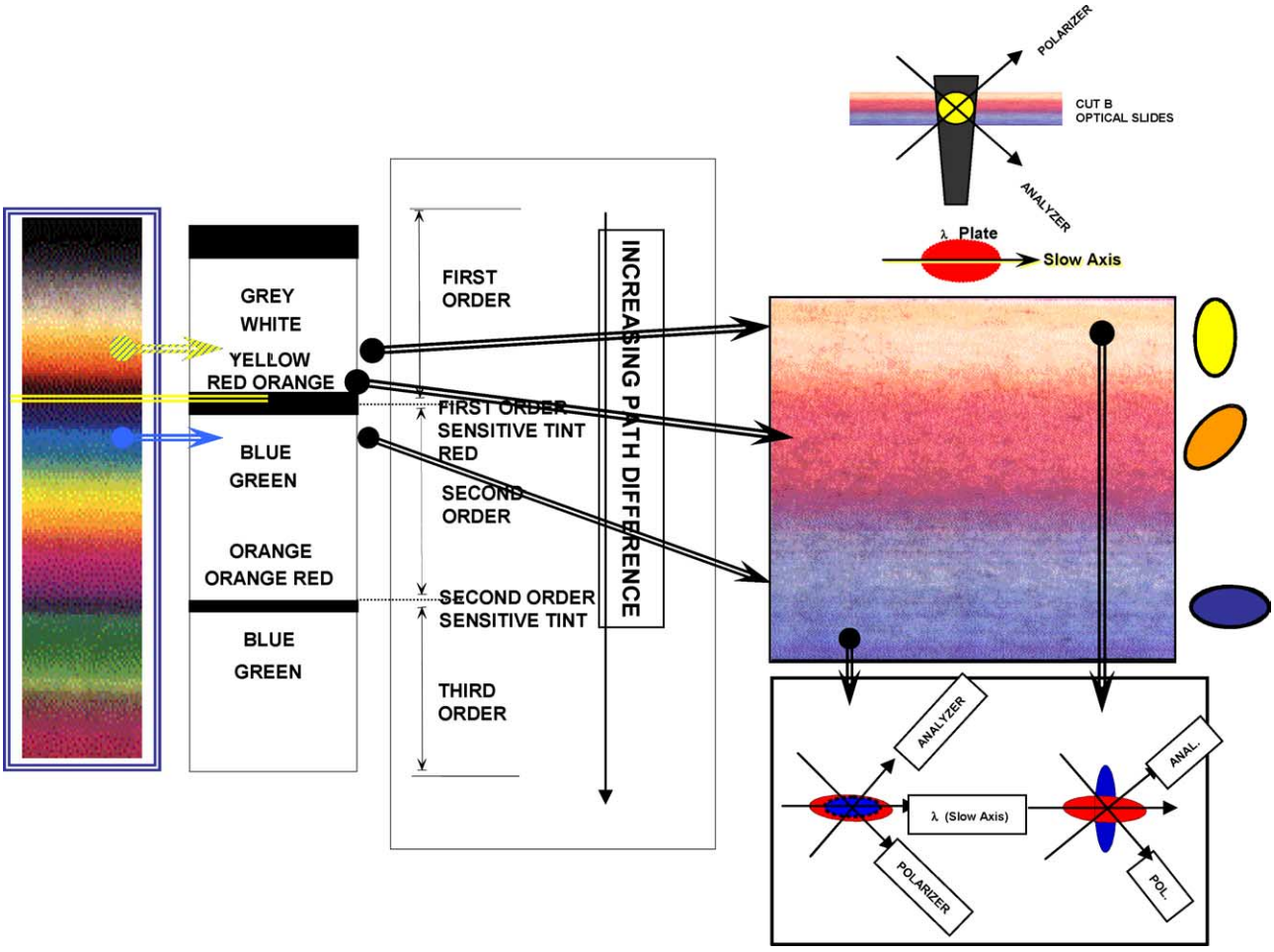

Fig. 10. Polarized optical microscopy of b-cut sample poly(3-hydroxybutyrate-*co*-hydroxyvalerate sample with first order red λ plate.

complex color sequences that are shown in Fig. 11. Those regions approaching isotropy would exhibit colors near the first order red tint and those regions that are substantially oriented would exhibit above mentioned colors depending on the orientation of their local symmetry axes relative to the slow axis of the lambda plate either in addition position (local slow axes are parallel to slow axis of the lambda plate) or subtraction position (the latter axes cross). These will be discussed together with Micro beam WAXS measurements below.

3.5. Birefringence

The birefringence of 5% HV, at high speed and 12% HV, at low and high injection speed are presented in Fig. 12, where the negative of the birefringence is shown. Birefringence first increases and show a maximum, then decreases toward the core region. For 12% HV, increasing the injection speed, decreases the birefringence from skin to core. The maximum in birefringence roughly coincides with the middle of the shear crystallized regions. These profiles are typical or what has been observed in injection molded parts in the past.

3.6. Microbeam WAXS study

In order to investigate the orientation behavior in the crystalline regions we obtained Micro beam X-ray patterns from skin to core at location #3 (midpoint of two end of the sample) using the cutting procedure B.

The samples were sectioned in FD–ND plane (B-cut), and mounted in a sample holder so that microbeam X-ray is directed along the normal of the FD (flow direction)–ND (normal direction) plane.

For 5% HV molded at low speed (Fig. 13), the (020) and (110) diffraction planes are primarily oriented in the normal direction throughout the thickness direction. We obtained azimuthal scans of (020) and (110) planes from these film patterns and determined the orientation factors for f_c (chain axis) f_b and f_a crystallographic directions. In this process the local symmetry axis was also determined and the local orientation factors were determined with respect to this local symmetry axis. In 5% HV sample, the local symmetry axis is oriented in the same direction as the Flow direction that is oriented vertically in the microphotograph. The *c*-axis orientation increases up to the middle of the blue section defining the shear region where maximum in

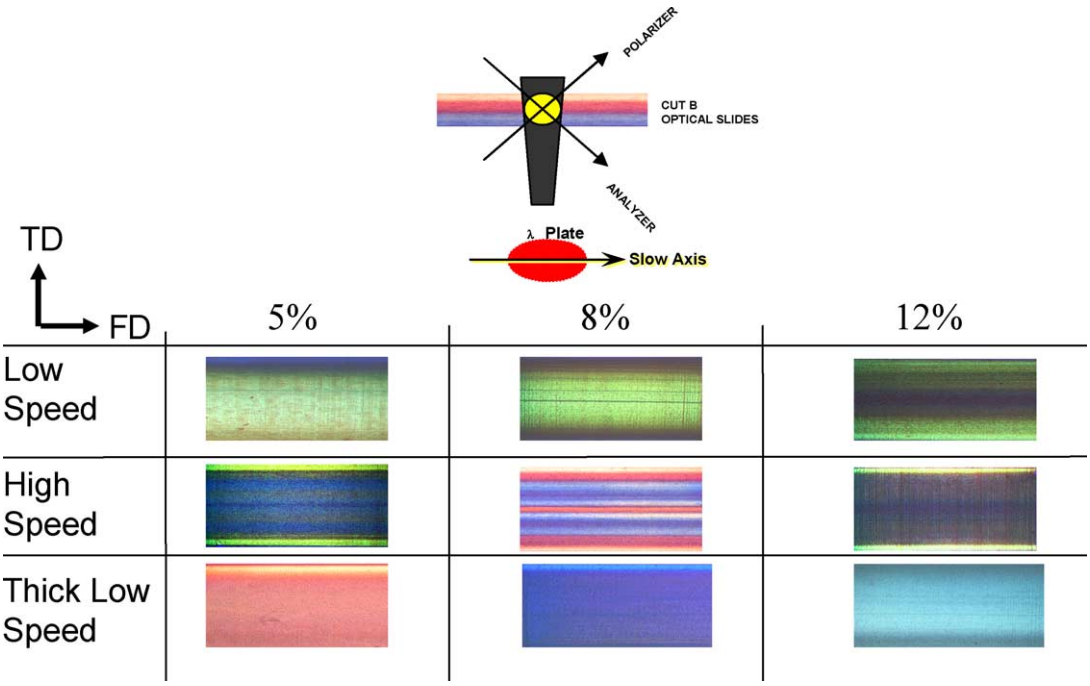

Fig. 11. B-cut optical microscopy of PHB/5, 8 and 12% HV for (a) thin low speed, (b) thin high speed, (c) thick low speed injection molded parts.

birefringence was also observed above, and decreases temporarily at the transition between the shear and the interior sections and following this systematically increase towards the core. It is quite surprising to observe that the core region exhibits the highest crystalline orientation compared to the skin regions. This is contrary to what is expected for fast crystallizing polymers such as polyethylene and polypropylene. This behavior similar to the orientation gradients observed in injection molded thermotropic liquid crystalline polymers that typically exhibit extremely long relaxation times and once oriented by the flow they remain in that state as shown by Hsiung, Jun and Cakmak [33,34]. We attribute this unusual behavior of PHBHV copolymers to the selection of melt processing temperature to very close to the end of the crystalline melting range. Under these conditions the flow stream coming from the injection unit would contain sizable fraction of unmelted crystals and/or freshly shear crystallized polymer coexisting with its own melt. This certainly would suppress the relaxation behavior in the interior of the parts after the stoppage of the flow.

Increasing the injection speed (Fig. 14) actually increases the skin and shear layer orientation and in the interior, this orientation gradually decreases particularly beyond the transition region with the curious behavior shown by the *fa* being positive indicating that the *a*-axis orientation along the flow direction begins to dominate while *c* and *b*-axes are oriented towards ND and TD directions in the samples.

Fig. 15, shows the X-ray and orientation data for 8% HV

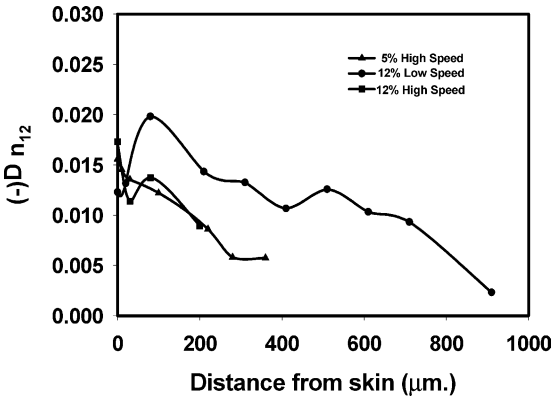

Fig. 12. Birefringence measurement of low speed 12%, high speed 5% and 12%.

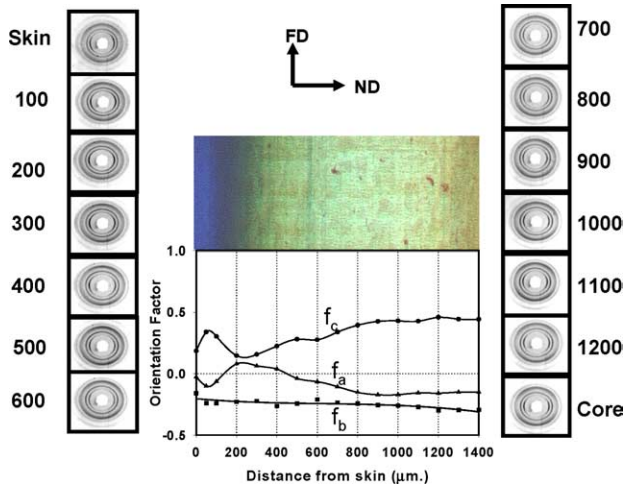

Fig. 13. Skin-core microbeam WAXS and orientation factors for low speed PHB-*co*-5% HV.

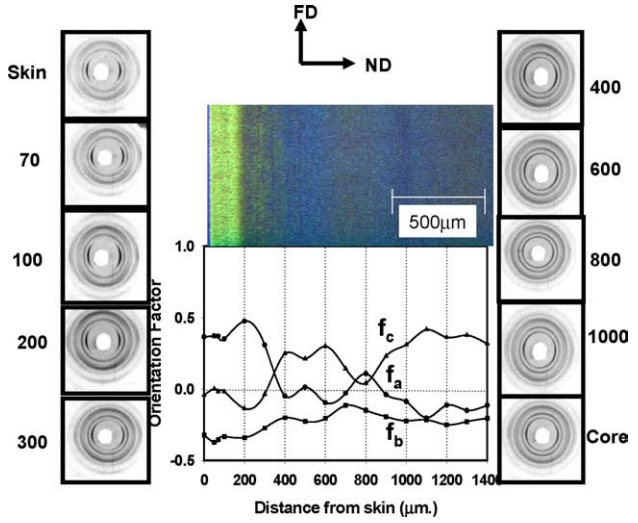

Fig. 14. Skin-core microbeam WAXS and orientation factors for high speed PHB-*co*-5% HV.

at low injection speed. In this sample the maximum in *c*-axis orientation is observed about 200 μm from the skin. Beyond this a rather complex behavior is observed including substantial local symmetry axis tilting associated with the flow behavior.

When injection speed is increased, the behavior is about the same as for low injection speed sample as shown in Fig. 16, exhibiting substantial local symmetry axis changes. These local symmetry axes are depicted with arrows on selected WAXS patterns and at the bottom of the figures representing their spatial distribution.

A completely different thickness dependency on the orientation is observed for 12% HV sample as shown in

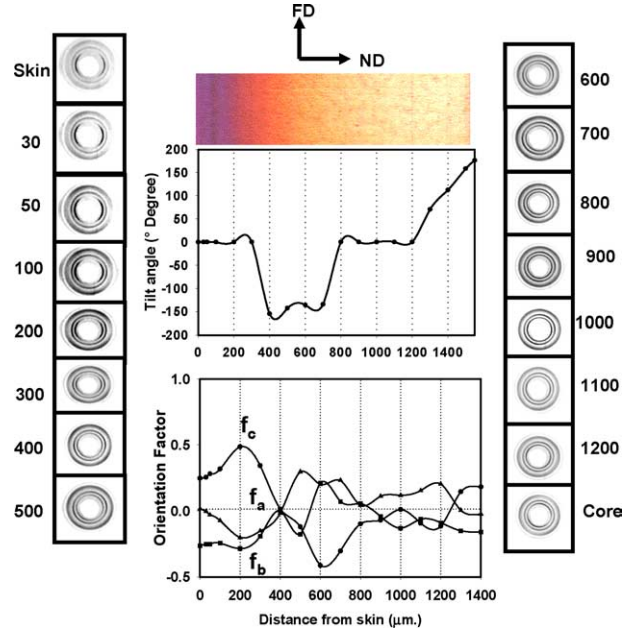

Fig. 15. Skin-core microbeam WAXS and orientation factors for low injection speed PHB-*co*-8% HV.

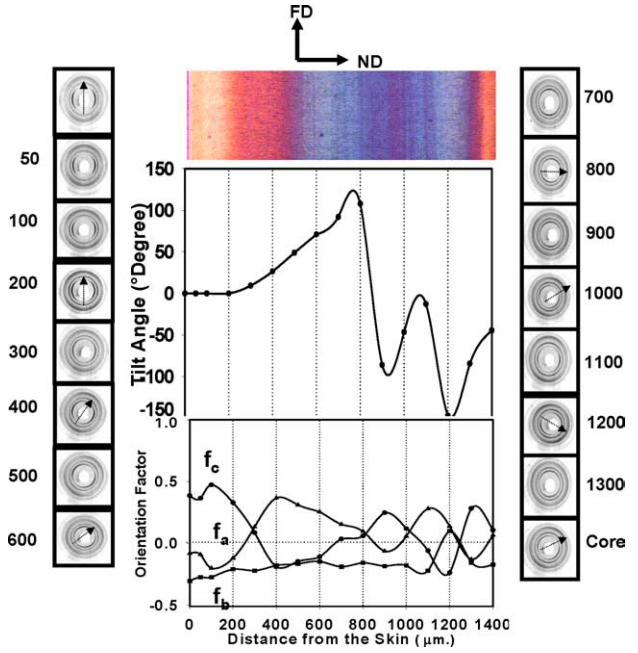

Fig. 16. Skin-core microbeam WAXS and orientation factors for high injection speed PHB-*co*-8% HV.

Figs. 17 and 18. This copolymer behaves in a behavior expected of semicrystalline polymer such as polyethylene [35] and polypropylene [36] PP/EPDM vulcanizates [37] and coinjection molded parts [38]. The surface region exhibit high orientation levels to about 500 μm towards the interior and the core is essentially unoriented. High speed injection actually leads to lower orientation levels as the oriented skin regions that formed during injection stage as a result of heat loss through the boundary become smaller as the filling stage becomes faster. This is also compounded by the fact that the melt temperature typically increases due to

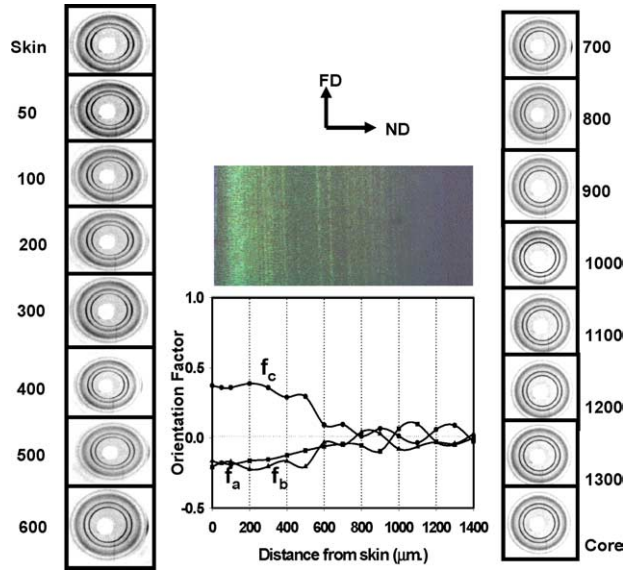

Fig. 17. Skin-core microbeam WAXS and orientation factors for low injection speed PHB-*co*-12% HV.

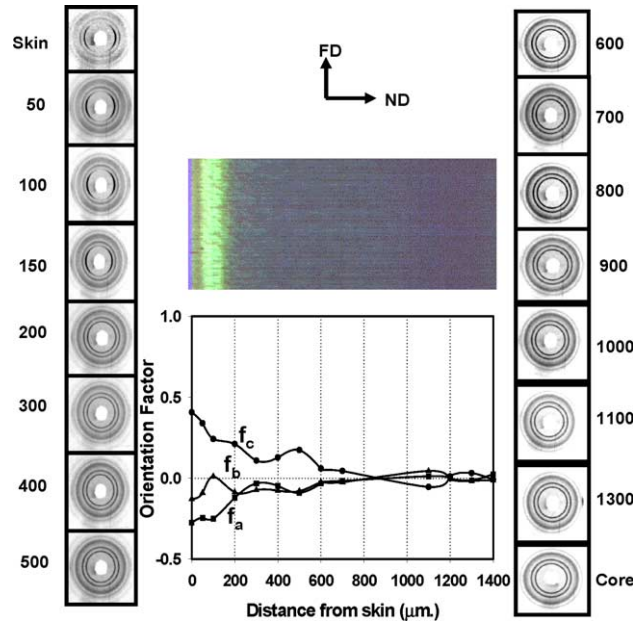

Fig. 18. Skin-core microbeam WAXS patterns and derived orientation factors for PHB-*co*-12% HV molded with high injection speed.

shear heating at higher injection speeds. Once the injection stage is completed however little orientation developed during the flow essentially relaxes away leaving the interior with little or no orientation. This is directly attributable to the widening the difference between the crystalline melting peak with 12% HV content processing temperature.

3.7. Effect of mold thickness on orientation behavior

As shown in Figs. 19–21 when the mold thickness is doubled, the 5% HV sample still exhibits orientation

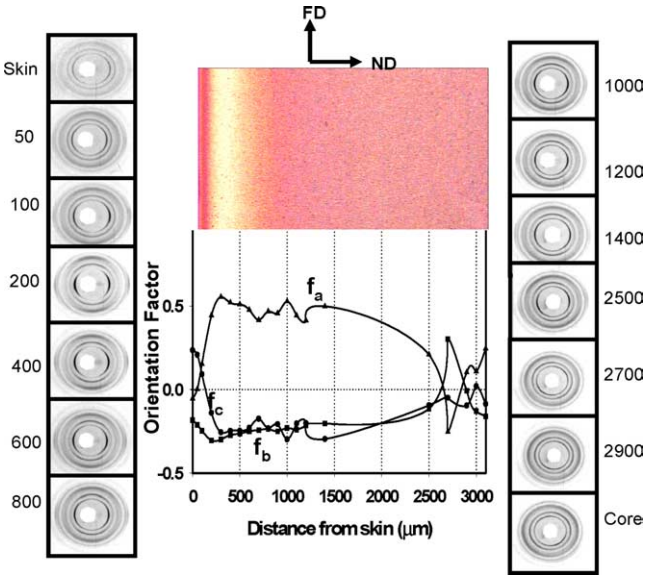

Fig. 19. Skin-core variation of microbeam WAXS patterns and derived orientation factors for PHB-*co*-5% HV rectangular sample injection molded with high injection speed.

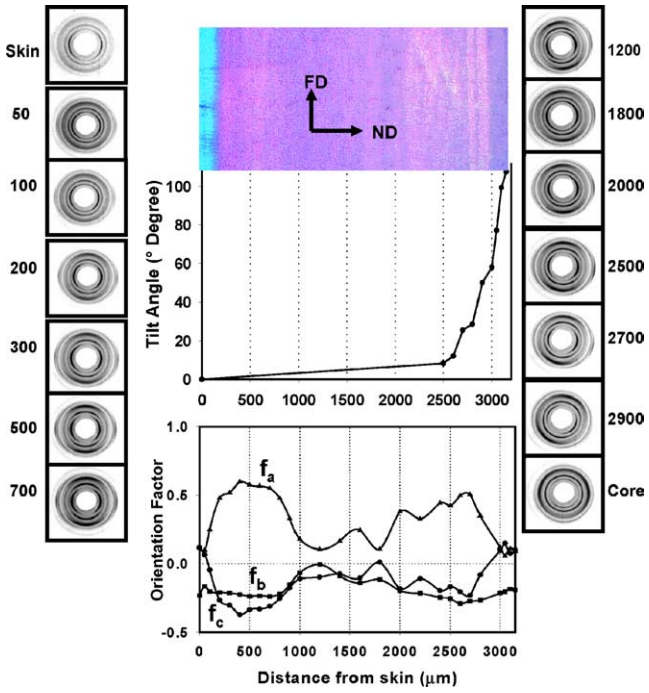

Fig. 20. Skin-core variation of microbeam WAXS patterns and derived orientation factors for PHB-*co*-8% HV rectangular sample injection molded with high injection speed.

behavior. Near the surface, the polymer chain axes are oriented in the flow direction but beyond the shear zone this quickly changes and the a crystallographic axes are oriented along the flow direction and this remains so for substantial portion of the sample.

For 8% HV sample (Fig. 20) we also observe similar behavior: a axes are primarily oriented in the flow direction while *c* and *b*-axes become oriented in the transverse direction especially near the surface. When the HV content is increased to 12% we observe effectively no orientation.

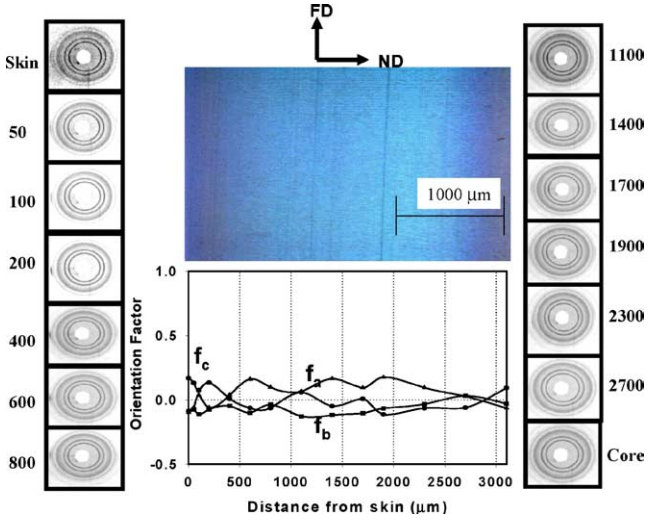

Fig. 21. Skin-core variation of microbeam WAXS patterns and derived orientation factors for PHB-*co*-12% HV rectangular sample injection molded with high injection speed.

3.8. WAXS pole figures

In order to asses the full texture in the crystalline regions in thick injection molded 8% HV sample we obtained WAXS pole figures for (020) and (110) planes at skin, intermediate levels (~1500 μm) and core (~3000 μm). These are shown in Fig. 22 for low speed and Fig. 23 for high speed injection.

As indicated earlier, upon injection the (020) planes become parallel to FD–TD planes (their poles become parallel to normal direction. While the (110) poles are roughly randomly distributed in the FD–TD plane this texture prevails throughout the thickness of the sample while the local symmetry axes show some deviations from the major sample axes (FD, TD, ND). A most remarkable feature of these pole figures is that even at the core of very thick sample (6 mm) substantial preferred orientation remains. Increase of injection speed does not alter the texture explained above. But at the core we observe the (020) poles are rotated towards the flow direction. This behavior presumably amplified during the packing stage where the polymer chains turn normal to the flow direction. This is a behavior akin to glass fiber orientation in the core regions of glass reinforced thermoplastics [39,40] or thermotropic liquid crystalline polymers. The *b*-axes are oriented primarily in ND and *a*-axes tend toward the flow direction with the end result the (110) planes show a distribution in FD–TD plane making the appropriate angle with the pole of (020) expected from the crystal structure.

3.8.1. Structural interpretations

Structural gradients developed in injection molded PHBHV are complex. However, we have established certain trends in the crystallization and orientation behavior of PHB/HV copolymers particularly with the influence of HV content in these random copolymers. In the literature it is well known that HV can easily be encapsulated by the HB crystals [28]. This is particularly true under rapid cooling conditions. However, if sufficient freedom to organize into most optimum configuration is provided, HV groups tends to congregate at the surface of the HB lamellae making them highly irregular and keeping their size small and hence their melting temperature becomes lower due to large surface energy contribution to specific enthalpy [29]. Our thermal analysis data indicate that the increase of HV content promotes this latter behavior, particularly at the interior of molded parts. However, at the skin regions we have observed that the there is a single, high temperature-melting peak with a large low temperature tail. The X-ray analysis of these region repeatedly has shown that the *c*-axis orientation is concentrated primarily in the flow direction. At these oriented layers we suspect that the crystal chain folding is greatly suppressed in forming extended chain crystals, thereby eliminating the possibility of HV segments to concentrate at the fold surfaces. Under these circumstances, the HV segments are incorporated into HB highly oriented crystals. The high melting peak arises from the large size of the crystals with certain level of defects formed under high shear/extensional flow that occurs near the skin while rapid

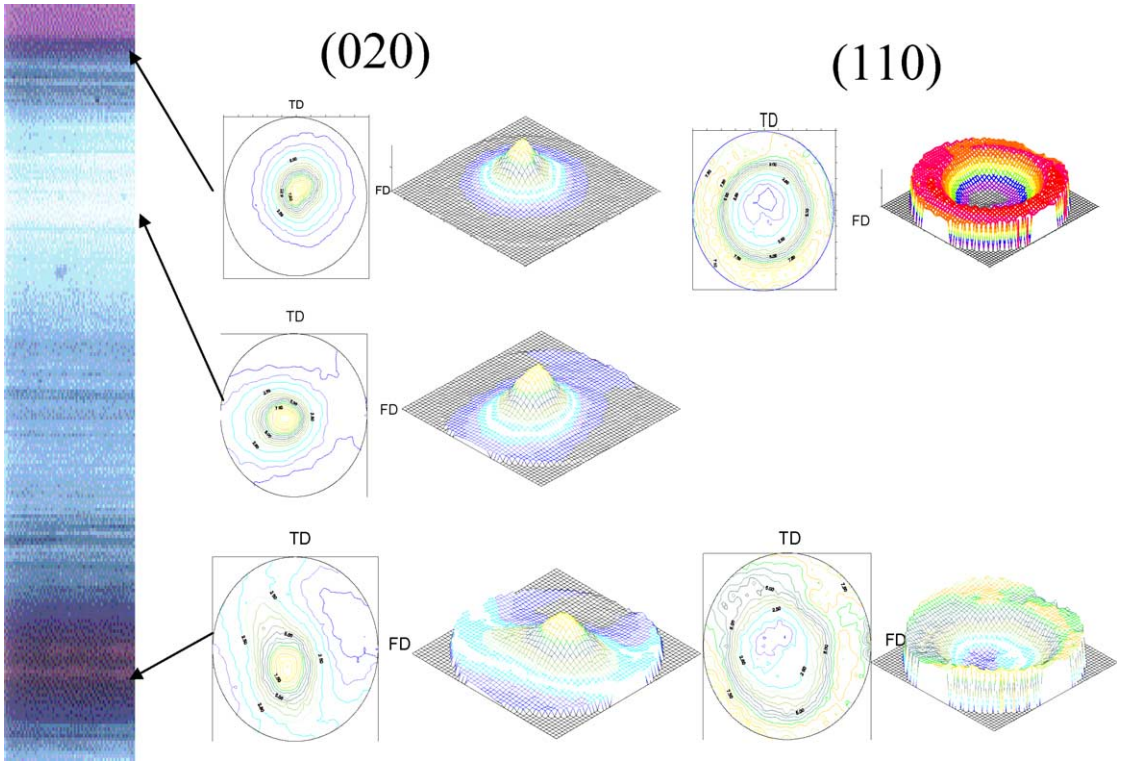

Fig. 22. Wide angle X-ray pole figure of (020) and (110) planes for 8% HV sample molded at low injection speed.

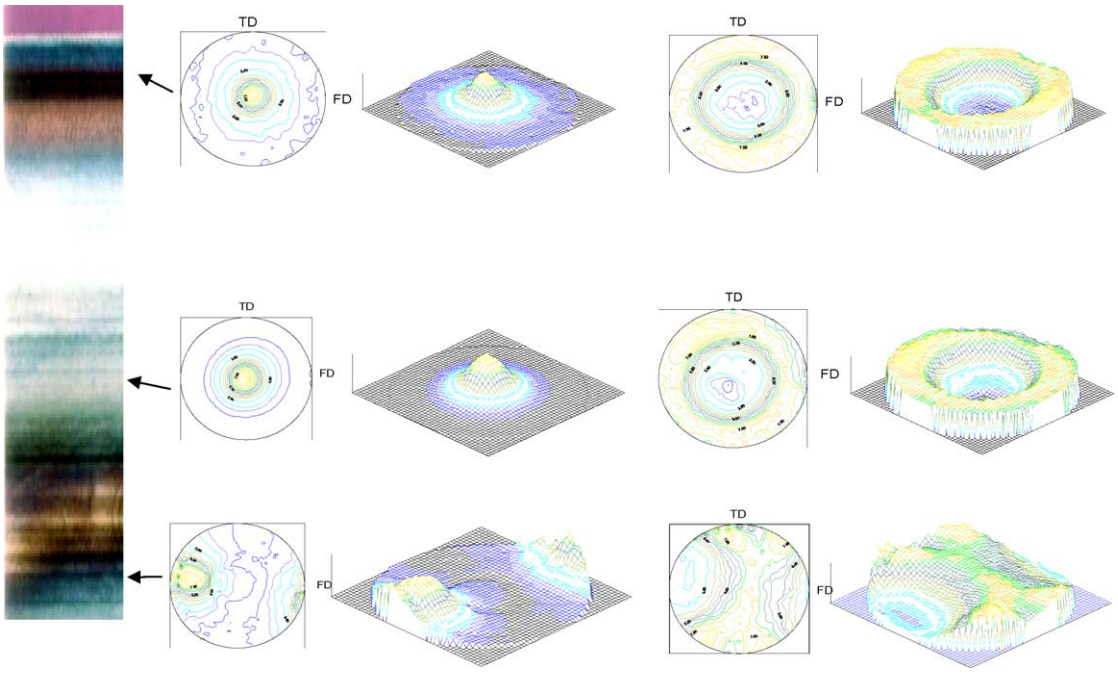

Fig. 23. Wide angle X-ray pole figure of (020) and (110) planes for 8% HV sample molded at high injection speed.

cooling takes place despite the fact that they contain HV defects. One of the other reasons we do not see a distinct lower temperature peak in the 5% and 8% HV is that their concentration is not adequate to create a separate population. Once the concentration reaches 12% HV we always observe a distinct lower melting peak even at the skin.

The fact that the lower melting population increases towards the core indicates that more of the HV segments are segregated into the interlamellar regions or at the surface of the lamellae forcing them to remain thinner, exhibiting lower melting temperatures. What is most remarkable is the observations of relatively strong crystalline chain orientations throughout the parts for 5% and 8% HV. In almost all of the samples the lower melting peak gradually begins to increase towards the core after showing a minimum value about half way between the skin and core. In the core we observe a single melting peak. This increase of melting peak is simply due to the slower cooling resulting in thicker lamellae despite the presence of HV defects.

In summary, the skin region is populated by the oriented extended chain crystals that contain significant amount of HV defects (responsible for broad low temperature tail of melting). At slightly interior locations the cooling rate slows down significantly enough to grow thin lamellar crystals with a small fraction HV defects in them but mostly on the surfaces of the lamellae. With the slowest cooling experienced in the core, these crystals gain sufficient time at higher temperatures to become larger and/or more perfect, resulting in increase of melting temperature.

Orientation of the crystalline regions exhibits a peculiar transition at a depth roughly corresponding to the boundary between the transition of shear layer to core regions. At the surface we observe *c*-axis oriented crystals along the flow direction as mentioned earlier. Beyond the transition layer the orientation does not disappear as was expected based on similar thermoplastics such as PE and PP but rather a change of orientation mode with *a*-axis oriented crystals (along the flow direction) mostly begin to dominate at the interior. This is particularly true for high injection speed as well as higher HV concentrations.

When 12% HV concentration is reached, the structural formation is entirely controlled by the crystallizability of the copolymer. The suppressed [41] crystallizability, as well as increased molten fraction in the melt stream, results in expected behavior from 12% HV. That is *c*-axis oriented crystals dominates near the skin and, as the distance from the surface increases, this orientation gradually disappears and core regions are found to be unoriented.

Increasing the mold thickness does not alter the overall orientation gradient observed in the thinner counterparts (*c*-axis orientation at the skin + even more pronounced *a*-axis orientation in the interior). However in these parts (5 and 8% HV in particular) the *a*-axis oriented crystal dominates almost all of part with the exception of very thin *c*-axis oriented skin regions. We did not see any significant orientation in 12% HV thick parts. Due to poor crystallizability this polymer simply could not maintain the preferred orientation developed during flow and it relaxed away before crystallization mechanism had a chance to lock it in.

Structural and Orientation models are presented in Fig. 24.

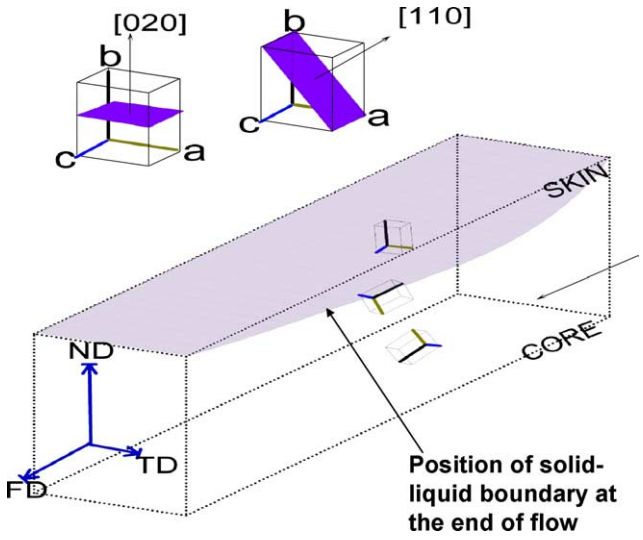

Fig. 24. Orientation behavior in PHB/HV copolymers.

4. Conclusions

Structural investigations using X-ray, optical and thermal analysis of PHB-*co*-HV with 5, 8 and 12% HV random copolymers revealed that these polymers exhibit two distinct orientation behaviors depending on the distance from surface. Those layers solidified during injection process exhibit *c*-axis orientation along the flow direction with the *b*-axis becoming parallel to the normal direction thus exhibiting uniplanar-axial texture. In these regions a single high melting peak with a large low temperature tail is observed and attributed to the oriented crystals that contain HV defects.

In the remainder of the interior of the samples that presumably solidified after injection we observed unusually high orientations all the way to core. This unexpected behavior from semicrystalline polymer is very similar to the behavior exhibited by those systems with little orientation relaxation behavior such as glass fiber filled thermoplastics as well as thermotropic liquid crystalline polymers. This orientation behavior is prevalent even in very thick molds. This suggests that the oriented crystals may have formed in high shear/extension flow regions upstream and retain that state during transportation down into their final positions in the mold as there is no local mechanism that would promote such level of orientations when considering the local flow processes. This is certainly facilitated by the fact that melt temperatures used in the process is unusually close to the crystalline melting range.

Upon increase of HV content to 12% in these random copolymers, we observe an expected behavior from a typical semicrystalline thermoplastic. Skin regions are *c*-axis oriented and beyond the transition the orientation disappears towards the core without showing any tendency to exhibit *a*-axis orientation. This clearly points that the relaxation plays a larger role in this polymer of substantially poorer crystallizability as well as due the absence of crystallites in the melt stream.

Acknowledgements

We would like to thank IIRI for financial support for one of us (T.Y.) to spend some time at University of Akron.

References

[1] Holmes PA. In: Bassett DC, editor. Development in crystalline polymers 2. New York: Elsevier; 1988.
[2] Dawes EA, Senior PJ. Adv Microbial Phys 1973;10:138.
[3] Wong PP, Evans HJ. Plant Physiol 1971;47:750.
[4] Merrick JM. In: Clayton Rk, Sistorm WR, editors. Potosynthetic bacteria. New York: Plenum; 1978. p. 199.
[5] Matin A, Veldhuis C, Stegman V, Veenhuis M. J Gen Microbiol 1979; 112:349.
[6] Skrbic Z, Divjakovic V. Polymer 1996;3:505.
[7] Ellar D, Lundgren DG, Okamuara K, Marchesslt RH. J Mol Biol 1968;35:489.
[8] Cornibert J, Marchessault RH. J Mol Biol 1972;71:735.
[9] Barham PJ, Keller A, Otun EL, Holmes PA. J Mater Sci 1984;19: 2781.
[10] Holmes PA, Wright LF, Collins SH. (Imperial Chemical Industries plc), Eur patent Appln EP 52459, 1981.
[11] Holmes PA, Wright LF, Collins SH. (ICI plc), Eur Patent appln, EP 69497, 1983.
[12] Pundsack A, Bluhm T. J Mater Sci 1981;16:545.
[13] Mitomo H, Barham PJ, Keller A. Polym J 1987;19:1241.
[14] Bluhm T, Hamer H, Marchesault H, Fyfe C, Veregrin R. Macromolecules 1986;19:2871.
[15] Marchessault R, Bluhm T, Deslands Y, Hamer G, Orts W, Sundararjan P, et al. Macromol Chem, Macromol Symp 1988;19:235.
[16] Skrbic Z, Divjakovic V, Petrovic Z. Polymer 1997;5:1239.
[17] Owen AJ, Heinzel J, Skrbic Z, Divjakovic V. Polym J 1992;33(7): 1563.
[18] Mitomo H, Barham PJ, Keller A. Seni-Gakkaishi 1986;42:T589.
[19] Organ SJ, Barham PJ. J Mater Sci 1991;26:1368.
[20] Wang YD, Yamamoto T, Cakmak MJ. J Appl Polym Sci 1996;61(11): 1957–70.
[21] Renstad R, Karlsson S, Albertsson AC, Werner P-E, Westdahl M. Polym Int 1997;43:201.
[22] Yamamoto T, Kimizu M, Kikutani T, Furuhashi Y, Cakmak M. Int Polym Process 1997;12I:29.
[23] Yamamoto T, Kimizu M, Kikutani T, Furuhashi Y, Cakmak M. Int Polym Process 1997;12(1):29–37.
[24] Hermans PH, Platzek P. Kolloid Z 1939;88:68.
[25] Wichinsky ZW. Advances in X-ray analysis. vol. 6. New York: Plenum Press; 1963. pp. 231.
[26] Wilchinsky ZW. J Appl Phys 1959;30:792.
[27] Keuchel K. MS Thesis, College of polymer Science and Polymer Engineering, University of Akron, 1994.
[28] Mitomo H, Takizawa T, Keller A. Sen-I Gakkaishi 1988;44:361.
[29] Owen AJ, Heinzel J, Skrbic Z, Divjakovic V. Polymer 1992;33:1563.
[30] Hsiung CM, Cakmak M, Ulcer Y. Polymer 1996;37(20):4555–71.
[31] Hsiung CM, Cakmak M. Coll Polym Sci Polym Eng, Polym Eng Sci 1991;31(19):1372–85.
[32] Takemura K, Koyama K, Kikutani T, editors. Plastic materials in polymer processing III textbook series on processing of plastics. Publisher Shiguma Syuppan.

[33] Hsiung CM, Tian J, Cakmak M. Inst Polym Eng, Univ Akron, Akron, OH, USA. Int Polym Process 1993;8(2):164–77.
[34] Hsiung CM, Cakmak M. Inst Polym Eng, Univ Akron, Akron, OH, USA. Int Polym Process 1993;8(3):255–70.
[35] Kamal MR, Moy FH. J Appl Polym Sci 1983;28(5):1787–804.
[36] Zhu P-W, Edward G. Polymer 2004;45(8):2603–13.
[37] Cakmak M, Cronin SW. Rubber Chem Technol 2000;73(4):753–78.
[38] Kadota M, Cakmak M, Hamada H. Polymer 1999;40(11):3119–45.
[39] Waschitschek K, Kech A, Christiansen JdeC. Department of production, Aalborg University, Aalborg, Den. Compos, Part A: Appl Sci Manufacturing 2002;33A(5):735–44.
[40] Larsen A. SINTEF. Polym Compos 2000;21(1):51–64.
[41] Mitomo H, Barham P, Keller A. Polym J 1987;19:1241.